Supplementary Information

Switching on SERS from SERS-Inactive Substrates through Simple Electrodeposition Guided by Defective Molecular Layer

Donghyeon Kim, Francisco García-González, Seunghun Lee, Juan C. Otero, and Mijeong Kang**

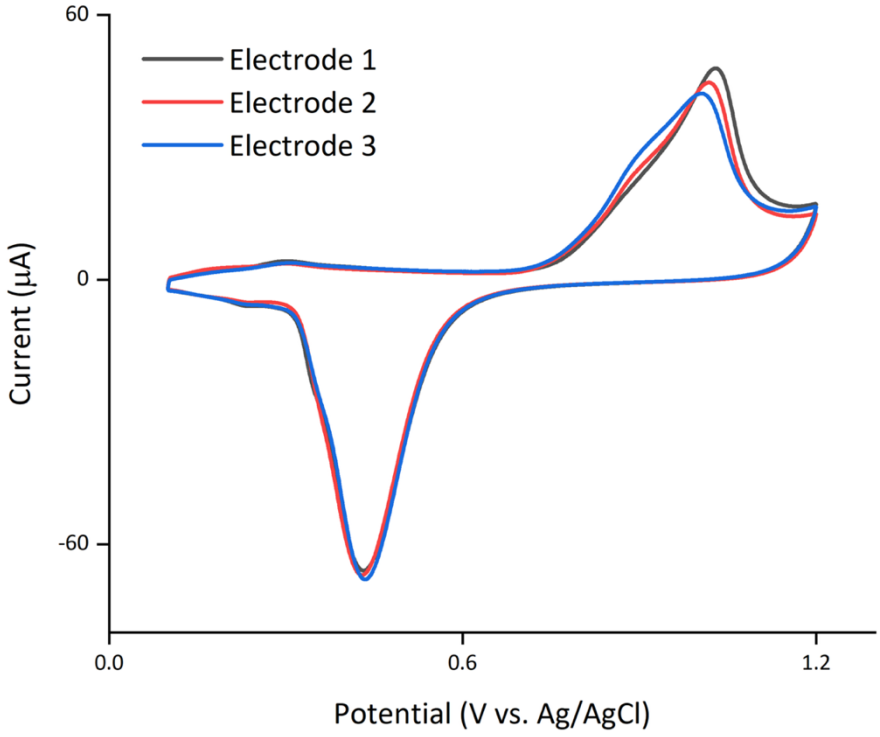

Figure S1. Cyclic voltammograms acquired during the electrochemical cleaning of three independent Au electrodes in a phosphate buffer solution. Cyclic voltammetry was performed over a potential range from 0.1 to 1.2 V (vs. Ag/AgCl) at a scan rate of 100 mVs^{-1}. The electrochemically active surface areas (EASAs) were calculated using the reduction current of Au oxides. The reduction peaks of the three Au electrodes are similar in current level, indicating that their EASAs are comparable. The average EASA was calculated to be 0.21 cm^2.

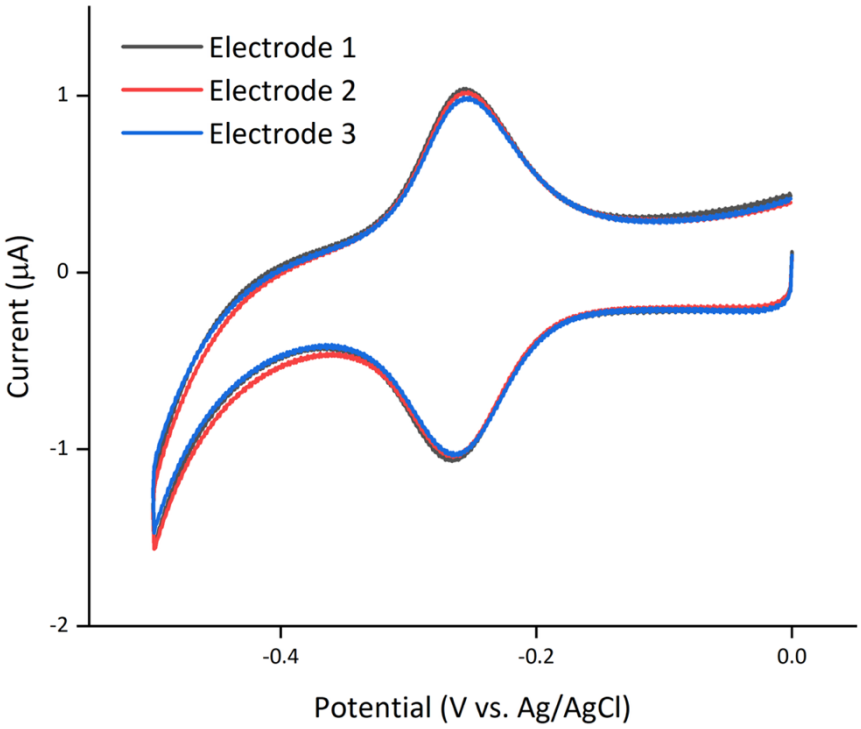

Figure S2. Cyclic voltammograms showing the reduction and oxidation peaks of the methylene blue (MB^+) from three independent Au electrodes modified with MB^+-labeled DNA strands and mercaptohexanol. Cyclic voltammetry was performed over a potential range from 0 to -0.5 V (vs. Ag/AgCl) at a scan rate of 100 mVs^{-1}. The comparable redox peaks of the MB^+ indicate that MB^+-labeled DNA strands are successfully immobilized on the three electrodes at comparable areal densities.

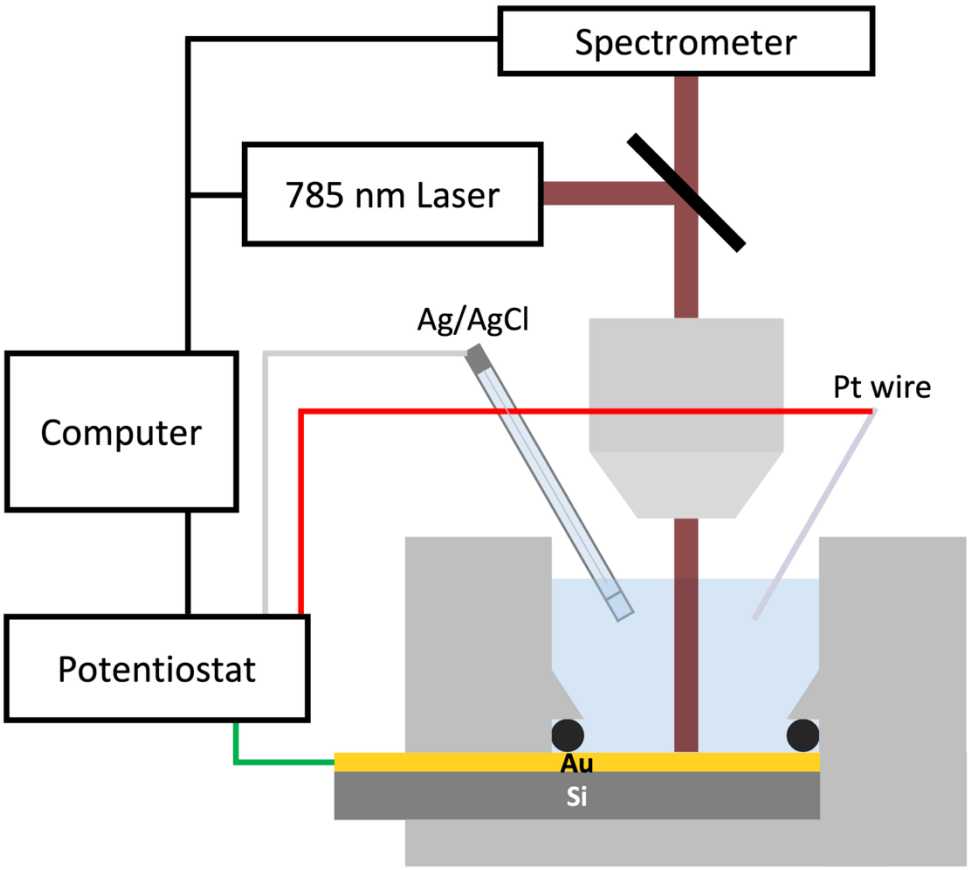

Figure S3. Schematic of the electrochemical surface-enhanced Raman scattering setup. A Au electrode is fixed in the cell and serves as a working electrode with a Ag/AgCl (3 M NaCl) reference electrode and a platinum counter electrode. The Raman spectrometer and potentiostat are connected to a single computer, and measurements are controlled simultaneously.

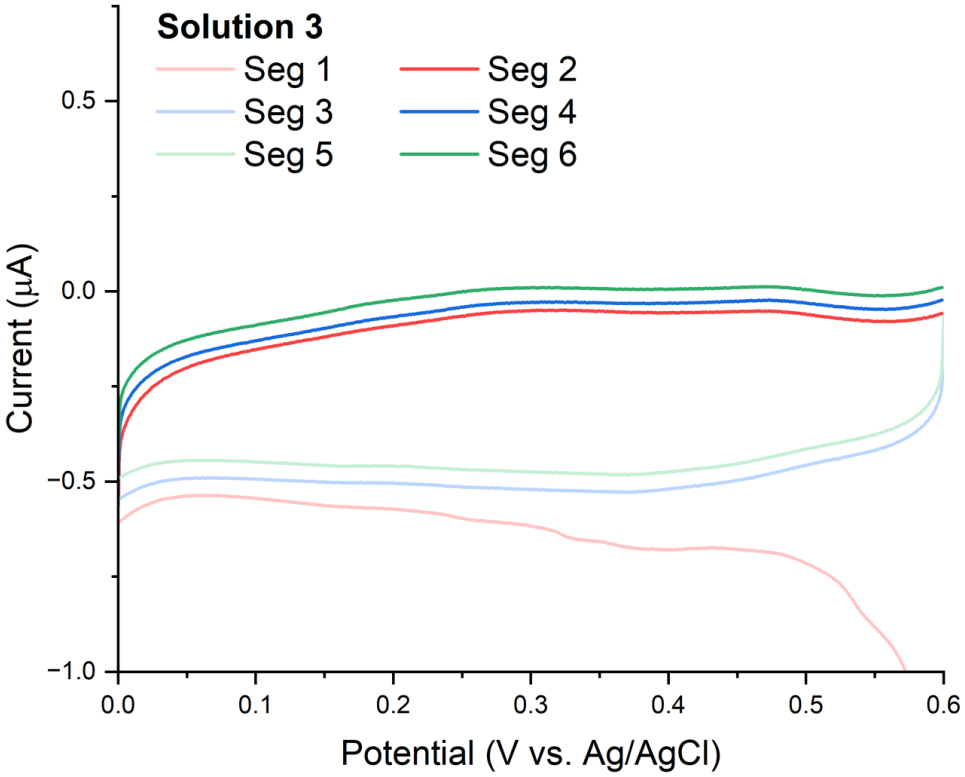

Figure S4. Enlarged cyclic voltammograms shown in Figure 2e.

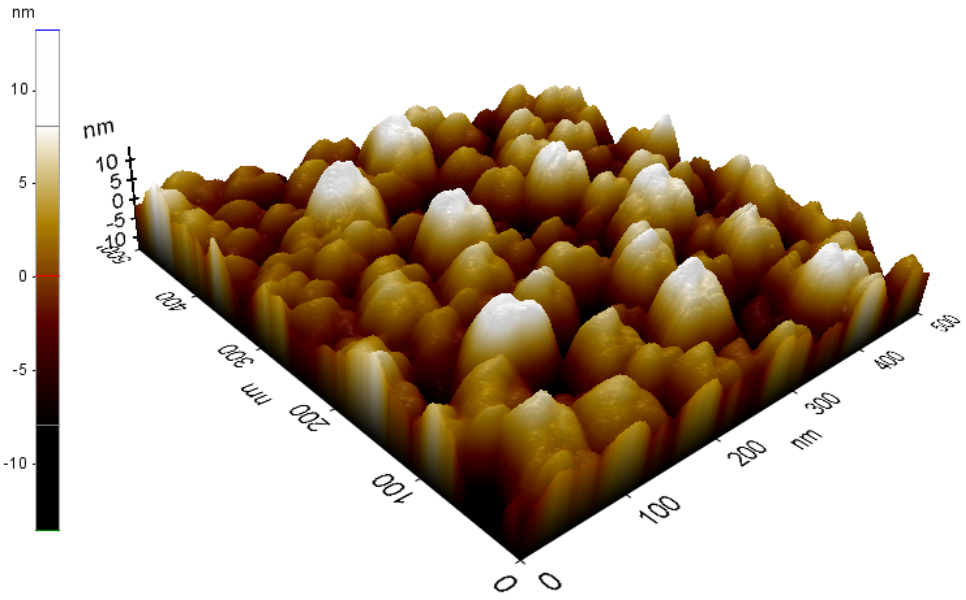

Figure S5. Three-dimensional atomic force microscopy image of the flat Au electrode surface. The electrode surface was first cleaned chemically (using a piranha solution) and then electrochemically. The average surface roughness was measured to be 0.669 nm.

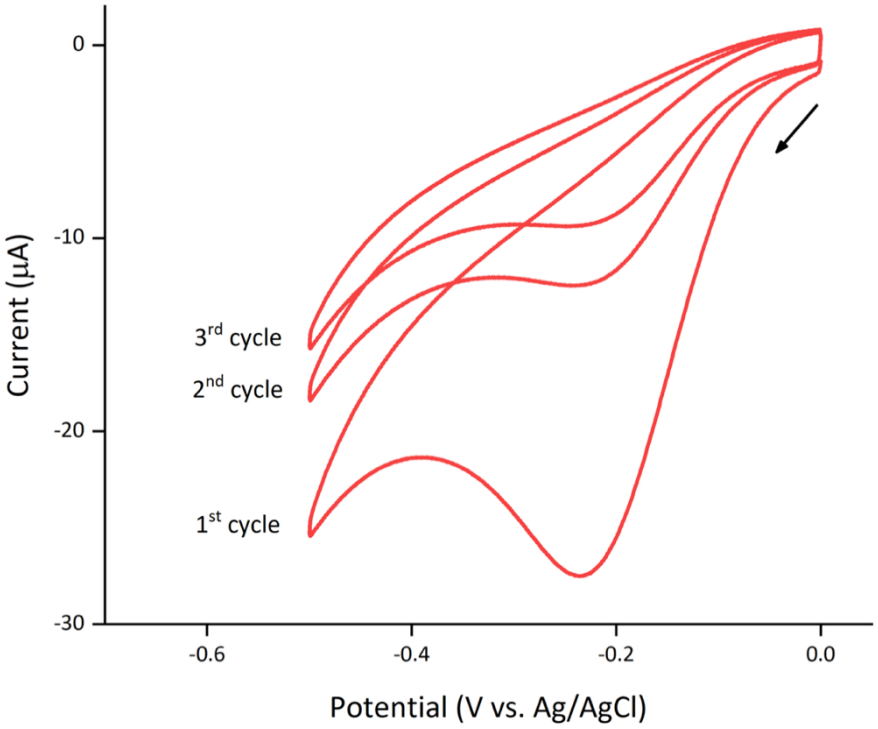

Figure S6. Cyclic voltammogram acquired using a bare Au electrode in a phosphate buffer solution. Cyclic voltammetry was performed over a potential range from 0 to −0.5 V (vs. Ag/AgCl). In this potential range, molecular oxygen (O_2) dissolved in the solution is reduced (i.e., undergoes oxygen reduction reaction). With repeating potential cycles, the dissolved oxygen is gradually consumed, resulting in a decrease of the corresponding reduction current.

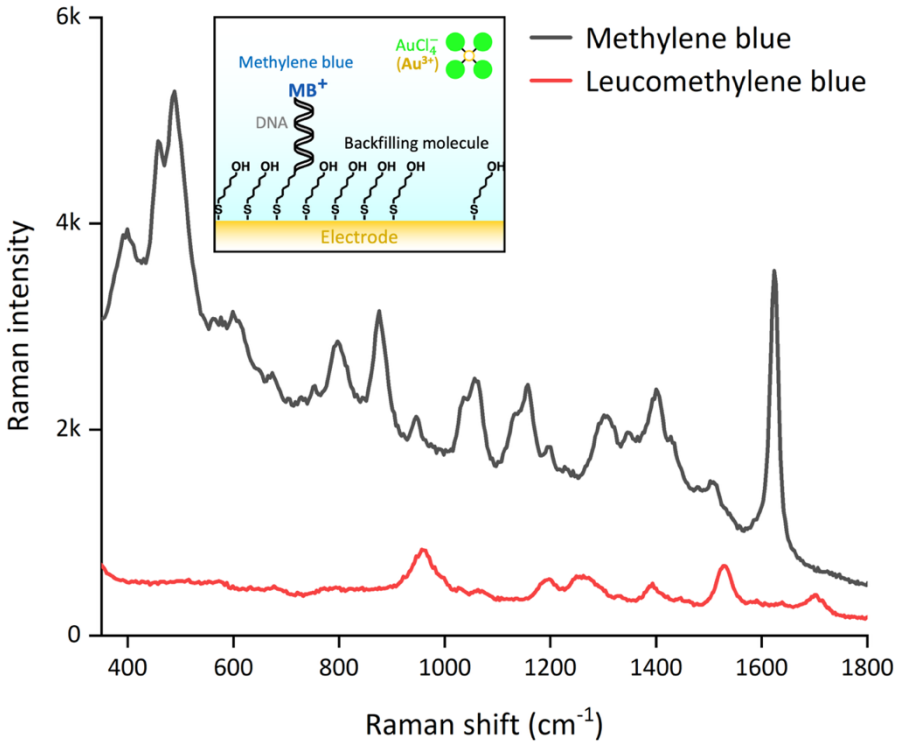

Figure S7. The electrochemical surface-enhanced Raman scattering spectra of methylene blue (MB^+) and its reduced species, leucomethylene blue (LMB). For this measurement, a Au electrode modified with MB^+-labeled DNA strands and mercaptohexanol was used, as illustrated in the inset schematic. The potential alternately sweeping between 0.75 V and -0.5 V (vs. Ag/AgCl) for three cycles was applied to the Au electrode in the presence of the $AuCl_4^-$. The Raman spectrum of MB^+ was obtained when the potential was 0.5 V in the second cycle, and that of LMB was obtained when the potential was -0.5 V in the second cycle. [Note: the formal reduction potential ($E^{\circ\prime}$) of MB^+ was determined from the the anodic and cathodic peak potentials shown in the cyclic voltammogram of Figure S2, which was -0.26 V (vs. Ag/AgCl).] For the LMB, the strongest Raman signal of MB^+ (1623 cm^{-1}) is not detectable.

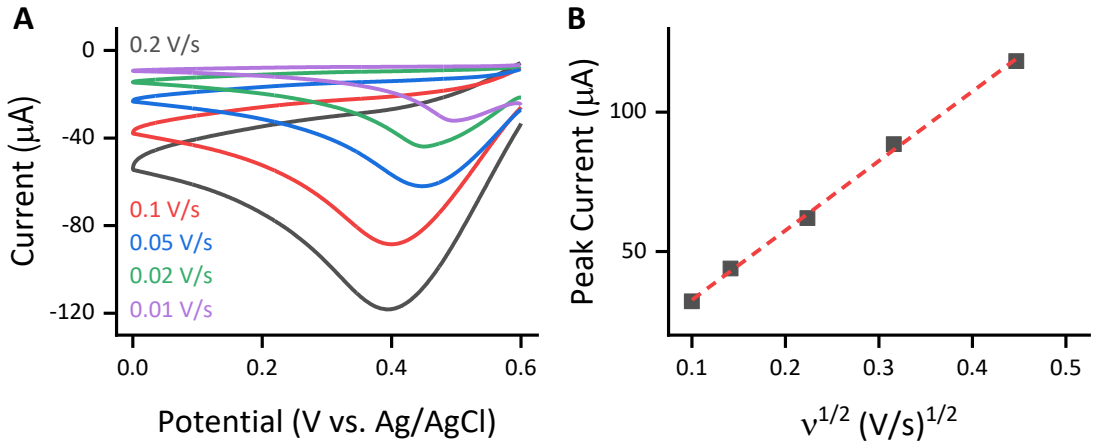

Figure S8. Effect of scan rate on the peak current in the cyclic voltammogram for the electrochemical reduction of $[AuCl_4]^-$. (a) Cyclic voltammograms recorded in a solution containing 1 mM $[AuCl_4]^-$ and 0.1 M NaCl at scan rates varying from 0.01 to 0.2 V/s. (b) Dependence of the reduction peak current of $[AuCl_4]^-$ on the square root of the scan rate, as extracted from the data shown in (a). ν denotes scan rate.

According to the Randles–Ševčík equation, if a redox reaction is electrochemically diffusion-controlled, the peak current observed in a cyclic voltammogram is proportional to the square root of the scan rate ($i_p = 0.4463nFAC(nF\nu D/RT)^{1/2}$, where ν is the scan rate). To examine this relationship for the reduction of $[AuCl_4]^-$, cyclic voltammetry measurements were carried out using a standard Au disk electrode under the same conditions as those employed in the EC-SERS experiments in Solution 2 (containing 1 mM $[AuCl_4]^-$ and 0.1 M NaCl) (Figure S8). The scan rates were varied from 10 to 200 mV s^{-1} (10, 20, 50, 100, and 200 mV s^{-1}), and the potential was swept from 0.6 to 0 V (vs. Ag/AgCl). In this potential range, $[AuCl_4]^-$ is reduced and deposited onto the electrode surface, leading to a gradual increase in the effective surface area of the electrode. Although this makes a rigorous quantitative analysis nontrivial, a clear linear relationship between the peak current and the square root of the scan rate was

nevertheless observed ($R^2 = 0.9982$). These results confirm that the reduction of $[AuCl_4]^-$ proceeds via a diffusion-controlled process.

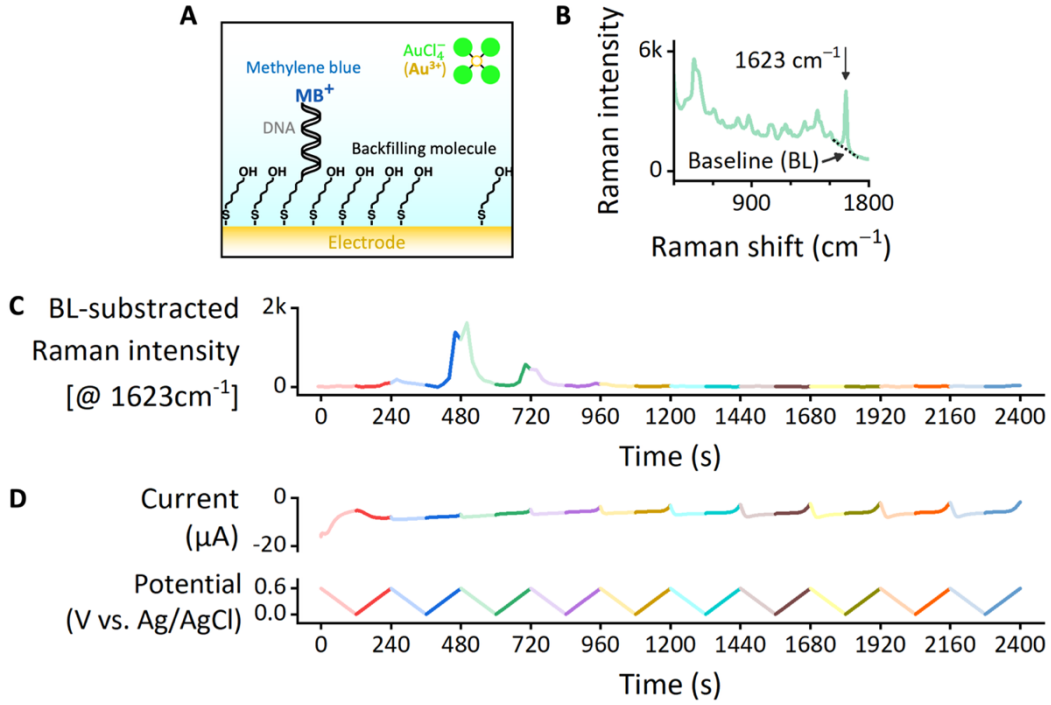

Figure S9. Electrochemical surface-enhanced Raman scattering (EC-SERS) for ten potential cycles. **A.** The surface of a Au electrode was modified with methylene blue (MB^+)-labeled DNA strands and mercaptohexanol. The EC-SERS was performed in the presence of $AuCl_4^-$ to electrodeposit the Au nanoparticles, forming hotspots. **B.** Representative Raman spectrum showing an intense Raman band at 1623 cm^{-1} and its baseline (BL). **C.** Variation of the BL-subtracted Raman intensity at 1623 cm^{-1} over time. **D.** Re-plotted cyclic voltammogram showing the variation in current in response to the alternately sweeping electrode potential between 0.6 V and 0.0 V (vs. Ag/AgCl) over time. The $AuCl_4^-$ in the solution was continuously reduced for the entire potential period.

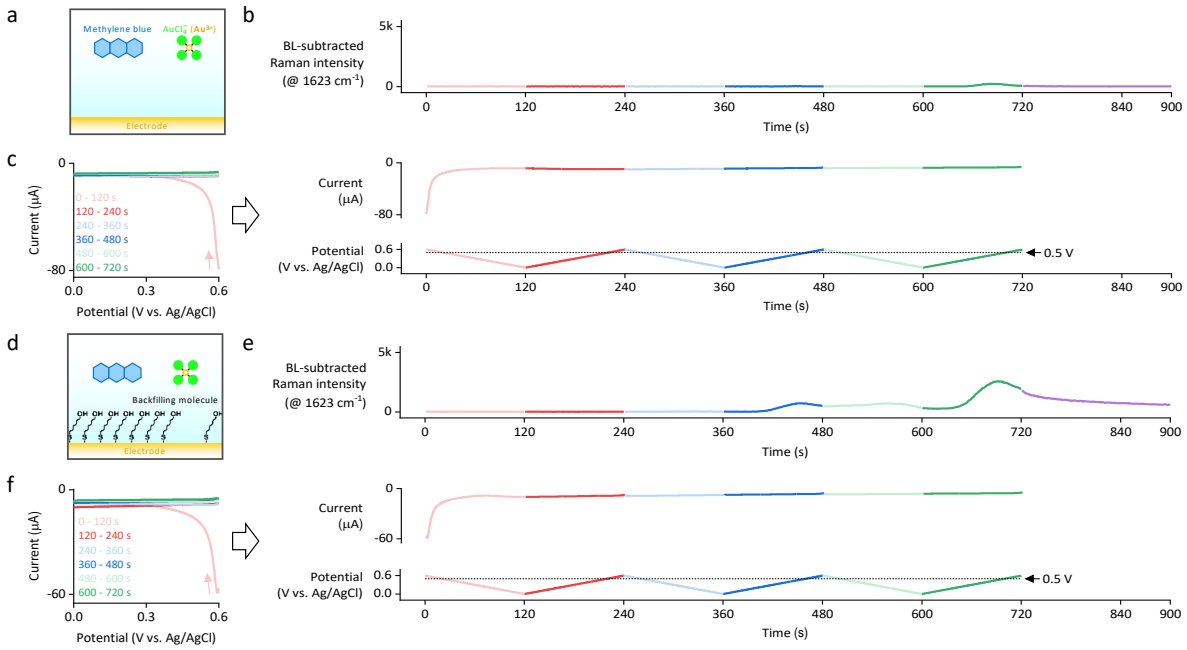

Figure S10. The investigation of the effect of a self-assembled monolayer on electrochemical surface-enhanced Raman scattering (EC-SERS) using a freely diffusing methylene blue (MB^+). **A.** Schematic of a bare Au electrode. **B.** Variation of the baseline-subtracted EC-SERS signal intensity at 1623 cm^{-1} over time in the absence of the simpler self-assembled monolayer (SAM). **C.** (Left) Cyclic voltammogram (CV) acquired during EC-SERS. (Right) Re-plotted CV showing the variation in current with varying the potential over time. **D.** Schematic of the mercaptohexanol (MCH)-coated electrode. **E.** Variation of the baseline-subtracted EC-SERS signal intensity at 1623 cm^{-1} over time in the presence of the simpler-SAM. **F.** (Left) CV acquired during EC-SERS. (Right) Re-plotted CV showing the variation in current with varying the potential over time.

Figures S10a–c show the electrochemical surface-enhanced Raman scattering (EC-SERS) results obtained from a bare Au electrode in a solution containing freely diffusible MB^+ molecules. Under these conditions, Au is expected to electrodeposit continuously on the electrode surface, as also evidenced by the scanning electron microscopy image of a bare Au electrode after electrodeposition shown in Figure 3d-ii. Such continuous Au deposition does

not lead to the formation of plasmonic hotspots; consequently, no effective enhancement of the Raman signal of MB^+ is observed.

In contrast, **Figures S10d–f** present the EC-SERS results obtained using a flat Au electrode modified with the self-assembled monolayer (SAM) of mercaptohexanol (MCH). Again, in this case, MB^+ molecules are freely diffusible in solution rather than immobilized at the end of DNA strands, as in the main text. Similar to the behavior observed in Figures 3c-i and 3c-ii, the presence of the SAM is expected to lead to discontinuous Au electrodeposition, thereby enabling the formation of effective plasmonic hotspots. As a result, the significant enhancement of the Raman signal of MB^+ is observed. These results demonstrate that even a simpler SAM, composed solely of MCH, is sufficient to enable effective EC-SERS on a flat Au electrode.

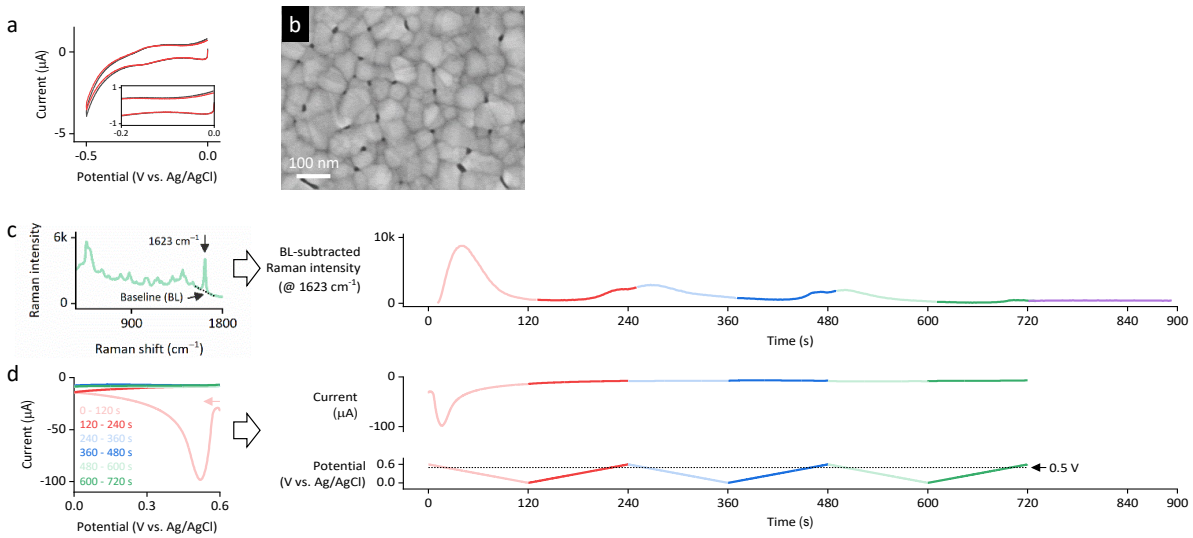

Figure S11. Effect of the quality of a self-assembled monolayer (SAM) on electrochemical surface-enhanced Raman scattering (EC-SERS). **A.** Cyclic voltammograms (CVs) acquired before (black) and after (red) the mercaptohexanol (MCH) assembly in a solution containing 0.1 mM MCH for 3 s. **B.** Surface scanning electron microscopy image of the electrode after EC-SERS. **C.** (Left) Representative EC-SERS spectrum showing a very strong signal at 1623 cm^{-1} and its baseline (BL). (Right) Variation of the BL-subtracted EC-SERS signal intensity at 1623 cm^{-1} over time. **D.** (Left) CV acquired during EC-SERS. (Right) Re-plotted CV showing the variation in current with varying the potential over time.

To verify that Au nanostructures preferentially form at defect sites of the self-assembled monolayer (SAM) of mercaptohexanol (MCH) and to further strengthen our proposed mechanism, we prepared Au electrodes with the SAM containing a higher density of defects and performed electrochemical surface-enhanced Raman scattering (EC-SERS) experiments. It is well established that SAMs composed of hydrocarbon-chain-based molecules require an appropriate molecular concentration and sufficient assembly time to form a compact and well-ordered monolayer (ref: Chem. Soc. Rev. 2010, 39, 1805). Based on this well-established understanding, a higher defect density was induced by lowering the MCH concentration and shortening the assembly time. Specifically, MB^+-labeled DNA–modified Au electrodes were

exposed to a 100 μM MCH solution for 3 s (for comparison, the condition reported in the main text involves immersion in a 5 mM MCH solution for 2 h) and then immediately rinsed with ethanol and deionized water.

The increased defect density of the electrodes prepared under the above conditions was confirmed by the enhanced capacitive current observed in cyclic voltammograms recorded in a blank buffer solution, as well as by the larger initial amount of Au deposited during the EC-SERS experiments. As shown in **Figure S11a**, when the MCH assembly time was very short (3 s), the capacitive current was slightly higher than that obtained with a much longer assembly time of 2 h. This increase is attributed to insufficient compactness of the SAM layer and/or an increased density of defects. The scanning electron microscopy image acquired after the EC-SERS experiments using the high-defect-density electrodes (Figure S11b) reveals that the electrodeposited Au islands have a higher connectivity than those formed on electrodes expected to have a lower defect density (Figure 3c-i). In Figure 3c-i, one side of the Au islands remains partially unfilled, leaving one-dimensional voids. In contrast, such one-dimensional voids are not observed in Figure S11b; instead, only smaller, zero-dimensional voids are present. This difference is likely due to the higher density of defects (i.e., a larger number of deposition-active sites) on the electrode surface, which promotes more extensive Au electrodeposition.

Furthermore, the variation of the EC-SERS signal obtained with the high-defect-density electrodes (**Figure S11c**) differs from that shown in Figure 2. In particular, a strong enhancement of the MB^+ Raman signal is observed already during the first potential cycle (for comparison, a strong enhancement is observed during the second potential cycle in Figure 2). We attribute this behavior to the increased number of SAM defects, which facilitates the formation of a larger number of Au nanoparticles at early stages, thereby increasing the

probability of hotspot formation in proximity to the MB^+ labels at the ends of DNA strands tethered to the electrode. This interpretation is supported by the observation that the reduction current associated with $[AuCl_4]^-$ in the first segment is approximately 2.57-fold higher than that reported in the main text (Figure 2). During the subsequent two potential cycles, the Raman enhancement gradually decreases as the Au nanostructures grow, consistent with the signal behavior shown in Figure S9. As the Au structures become larger, their effectiveness as plasmonic hotspots is partially decreased, leading to reduced Raman enhancement. Overall, by deliberately introducing a higher density of SAM defects, we modulated the defect-dependent Au electrodeposition behavior, thereby influencing the formation of the base Au electrode–MB^+-labeled DNA–electrodeposited Au layer hotspot architecture and, consequently, the EC-SERS response.

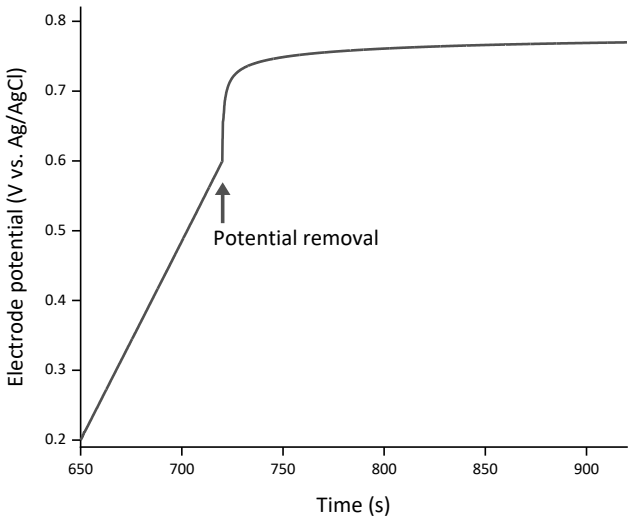

Figure S12. Time-dependent variation of the electrochemical potential between the Au working electrode and the reference electrode during the EC-SERS experiment in Solution 2, measured using a multimeter independent of the potentiostat. The potential applied by the potentiostat was disconnected at t = 720 s.

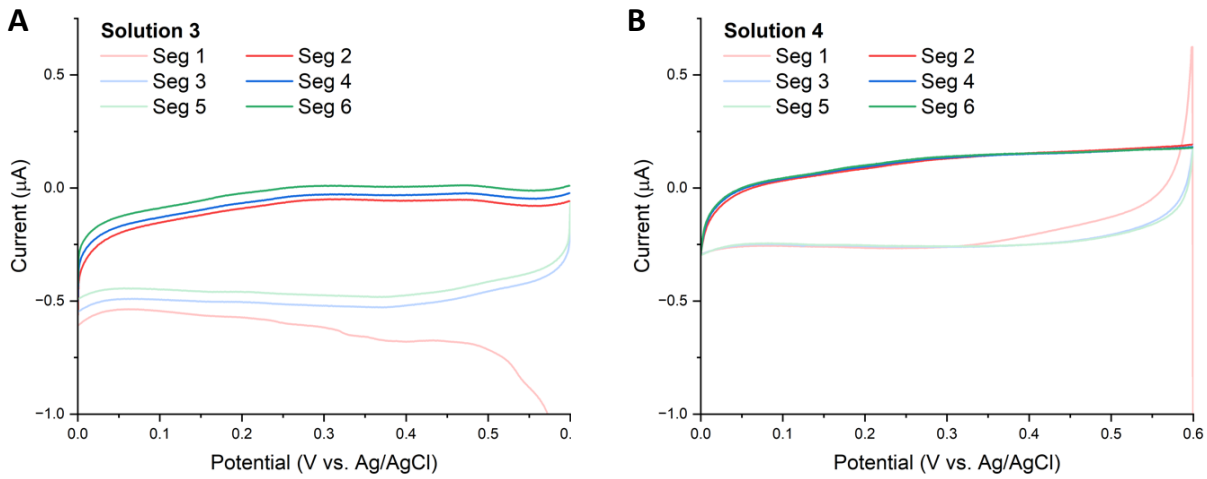

Figure S13. Enlarged cyclic voltammograms shown in Figures 4d and 4e.

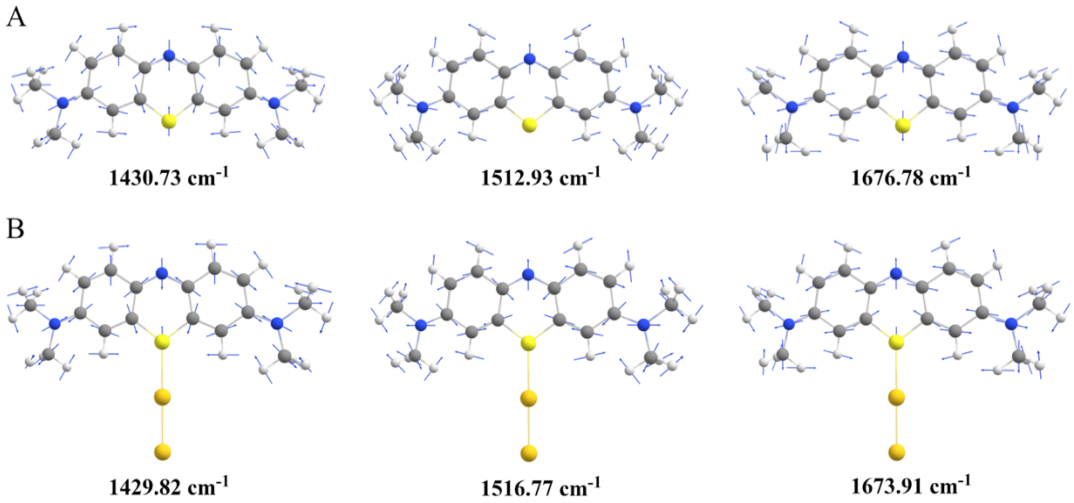

Figure S14. Vectors for the three most relevant electrochemical surface-enhanced Raman scattering (EC-SERS) vibrational modes for MB^+ (A) and Au_2MB^+ (B). B3LYP/6-31+G(d,p) level of theory for A and B3LYP/6-31+G(d,p)/LANL2DZ level of theory for B.

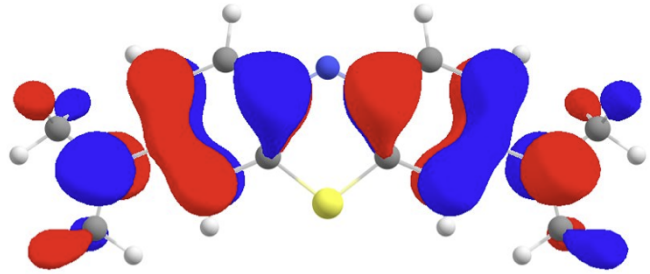

HOMO MB

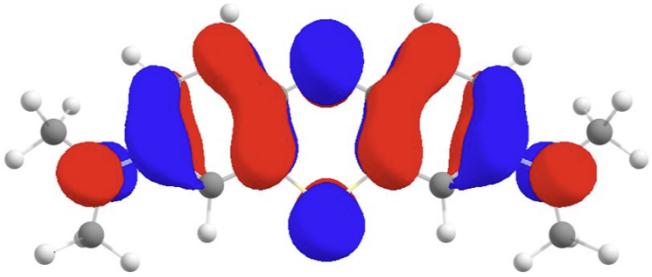

LUMO MB

Figure S15. Highest occupied molecular orbital (HOMO) and lowest unoccupied molecular orbital (LUMO) involved in the S_0-S_1 electronic transition of MB^+. B3LYP/6-31+G(d,p) level of theory. Surface isovalue of 0.03 e/bohr^3.

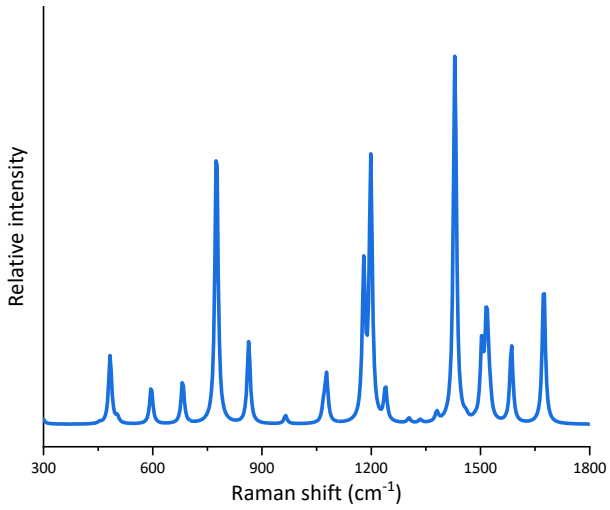

Figure S16. Calculated FC|VH resonance Raman spectrum obtained using density functional theory (DFT) and time-dependent DFT for Au_2MB^+ in resonance with its first metal-to-molecule resonant charge transfer (CT) excited state (S_1) with the excitation state of 1.9 eV.

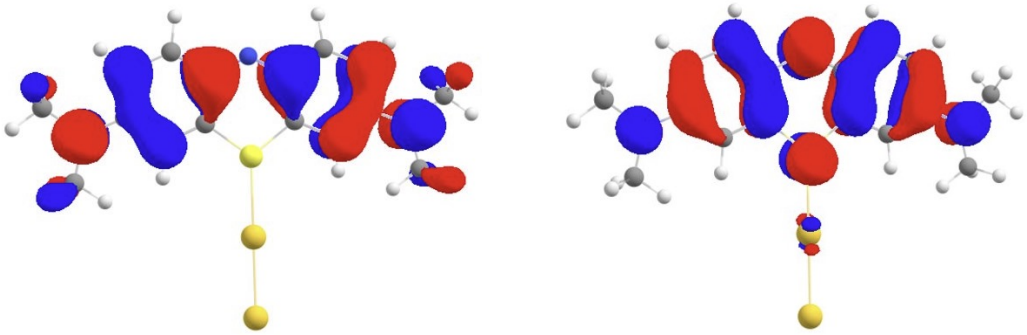

HOMO-1 Au_2MB **LUMO Au_2MB**

Figure S17. Second highest occupied molecular orbital (HOMO-1) and lowest unoccupied molecular orbital (LUMO) involved in the S_0-S_2 electronic transition of Au_2MB^+. B3LYP/6-31+G(d,p)/LANL2DZ level of theory. Surface isovalue of 0.03 e/bohr^3.

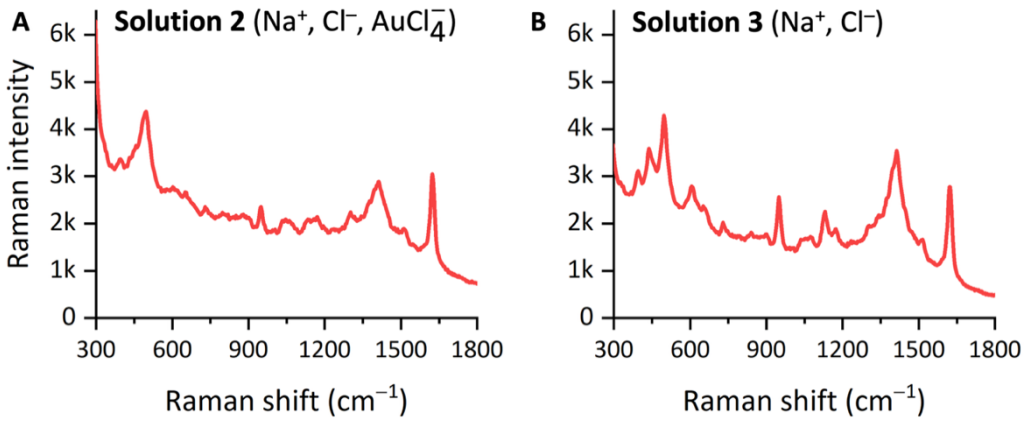

Figure S18. Investigation of the effect of chemical environments on the surface-enhanced Raman scattering (SERS) signals by simply changing the solution compositions. **A.** SERS spectrum acquired 5 minutes after the potential removal in Solution 2 (Na^+, Cl^-, $AuCl_4^-$). **B.** SERS spectrum acquired before the potential application in Solution 3 (Na^+, Cl^-). Simple removal of $AuCl_4^-$, without any potential application, induced the impressive change of EC-SERS spectra. The removal of $AuCl_4^-$ in Solution 3 induced a stronger 1412 cm^{-1} band compared to the 1623 cm^{-1} band.

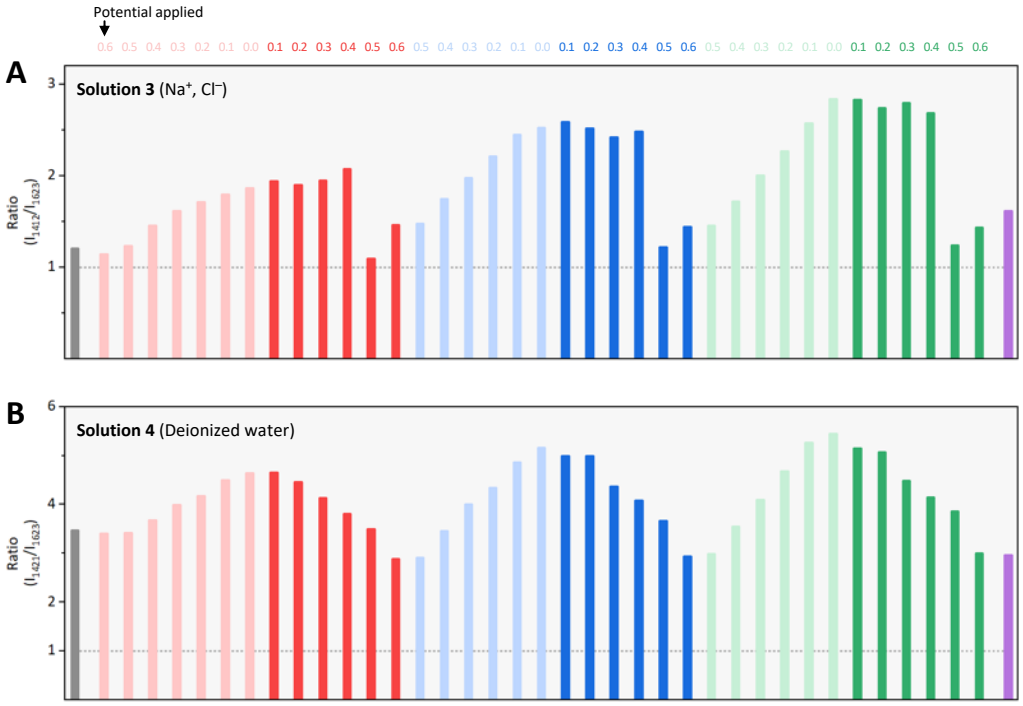

Figure S19. Enlarged intensity ratios of the ca. 1400 cm^{-1} bands to 1623 cm^{-1} bands shown in Figure 5.